

Electrostimulation as a prosthesis for repair of information flow in a computer model of neocortex

Cliff C. Kerr

Dept. of Physiology & Pharmacology, SUNY Downstate
School of Physics, University of Sydney
Sydney, NSW 2050, Australia
Email: cliffk@neurosims.downstate.edu

Samuel A. Neymotin

Joint Biomedical Engineering Program
SUNY Downstate & NYU-Poly
Brooklyn, New York 11203

George L. Chadderdon,
Christopher T. Fietkiewicz,
and Joseph T. Francis

Dept. of Physiology & Pharmacology, SUNY Downstate
Brooklyn, New York 11203

William W. Lytton

Dept. of Physiology & Pharmacology
SUNY Downstate & Kings County Hospital
Brooklyn, New York 11203

Abstract—Damage to a cortical area reduces not only information transmitted to other cortical areas, but also activation of these areas. This phenomenon, whereby the dynamics of a follower area are dramatically altered, is typically manifested as a marked reduction in activity. Ideally, neuroprosthetic stimulation would replace both information and activation. However, replacement of activation alone may be valuable as a means of restoring dynamics and information processing of other signals in this multiplexing system. We used neuroprosthetic stimulation in a computer model of the cortex to repair activation dynamics, using a simple repetitive stimulation to replace the more complex, naturalistic stimulation that had been removed. We found that we were able to restore activity in terms of neuronal firing rates. Additionally, we were able to restore information processing, measured as a restoration of causality between an experimentally recorded signal fed into the *in silico* brain and a cortical output. These results indicate that even simple neuroprosthetics that do not restore lost information may nonetheless be effective in improving the functionality of surrounding areas of cortex.

October 7th, 2011

I. INTRODUCTION

The term diaschisis, coined by von Monakow a century ago, describes remote effects of cortical damage resulting from loss of inputs to areas that are themselves undamaged [1]. Typically, diaschisis will reduce activity in the remote area due to the loss of the excitatory projections, although one might instead see increased activation in cases where these long-range excitatory projections synapse primarily on feedforward inhibitory interneurons [2]. The term has now further expanded to encompass a variety of remote effects, including vasogenic and humoral factors [3]. In this paper, we focus solely on the classical effect of loss of drive resulting in activity reduction, called here primary diaschisis.

While most brain projections involve some transfer of information, they also involve transfer of other signals, loosely

characterized as a drive or as a carrier signal. This dual nature of brain signaling can explain the surprising success in using nonspecific signals to replace lost specific signals. Most dramatically, systemic L-dopa provides a slowly-varying level of the neurotransmitter dopamine, yet effectively replaces the rapid pulsatile and location-specific natural neurotransmission that is lost in Parkinson's disease [4]. Similarly, deep brain stimulation (DBS) uses a nonspecific signal that can nonetheless change movement patterns to reduce tremor or dyskinesia [5]. In the sensory realm, phantom limb pain can sometimes be ameliorated by deep brain stimulation in somatosensory thalamus [6].

While the local organization of neocortical columns remains controversial (the very term column is disputed), there is some agreement on the general organization of inter-area connectivity patterns [7]. Sensory systems are organized in a hierarchy from primary areas that receive direct inputs via relay from the thalamus, through a wide variety of intermediate areas with various degrees of subspecialization, up to higher areas that integrate large amounts of information [8]. Although there are many cross-connections that complicate this scheme [9], we can generally speak of lower and higher areas, with a *forward* direction from primary sensory on up, and a *backward* direction starting in frontal and prefrontal areas responsible for attention. Projections in the forward direction emerge from the supragranular layer (layer 2/3) and project to granular (4) and infragranular layers (5 and 6). These projections convey primary sensory information such as proprioception, temperature, and touch in the somatosensory system. Projections in the backward direction primarily emerge from layer 5 and project to layer 2/3 of the more primary area [7]. These projections are believed to modulate attentional and binding influences that “tell” lower areas how to organize and focus their computational resources.

We hypothesize that it will be possible to repair the effects

of primary diaschisis by direct replacement of lost activity through electrical stimulation. In the case of the missing input from the forward pathway (loss of primary sensory input), this will involve stimulation of excitatory afferents to layer 4, while for the backward pathway (loss of higher or frontal areas), this involves stimulation of afferents to layer 2/3. As in the case of dopamine or DBS, the simple prosthetic stimulus replacements used here will not replace lost information but only attempt to restore other aspects of local processing. The first and most obvious restoration target is activity itself – spiking in the affected area. Subsequently, we look at whether our prosthetic stimulation can also repair more sophisticated dynamical relationships that might be expected to relate to information processing in neocortex.

We simulated an area of higher sensory or association cortex. Such an area will receive a number of different cortico-cortical inputs. We focus on two such inputs: the forward input from primary sensory areas that comes into layer 4 and the backward input from higher (more frontal) areas that project into layer 2/3. Generally, the layer 4 projection will bring in primary sensory information, while the layer 2/3 projection will provide directional or attentional information from areas privy to additional information. Hence, we damaged the inputs to the model that correspond to these two different major projection inputs, as shown in Fig. 1. Replacement was performed by adding input to the damaged areas by means of a neuroprosthesis generating a regular (i.e., single-frequency) input signal; thus, the signal from the prosthesis lacked the information content of the original. The goal of the prosthesis was to normalize dynamics.

II. METHODS

A. Experimental procedure

All animal procedures were approved by SUNY Downstate Medical Center IACUC and conformed to National Institutes of Health guidelines. A female Long-Evans rat (Hilltop, Scottsdale, PA) was anesthetized with isoflurane. Once a surgical level of anesthesia was obtained, as determined by the lack of any withdrawal reflex to a painful foot pinch, the rat was placed on a heating pad, the head was mounted onto a stereotaxic frame (Kopf Instruments, Tujunga, CA), and a craniotomy was performed. A 2x8-channel microelectrode array (MicroProbes, Gaithersburg, MD) was placed in the VPL nucleus of the thalamus, targeted to a location identified in a previous study [10] as having responses to cutaneous single-digit stimulation. The local field potential (LFP) used to drive the model consisted of 90 s of continuous data recorded from a single electrode, filtered using a 3rd-order Butterworth bandpass filter with cutoffs at 5 and 200 Hz.

B. Model

The model aims to describe the dynamics of a small region of primate sensory cortex. It is comprised of 4700 neurons divided into three types (excitatory pyramidal cells E , inhibitory interneurons I , and low-threshold spiking interneurons IL), distributed across the six layers of the cortex, for 13 distinct

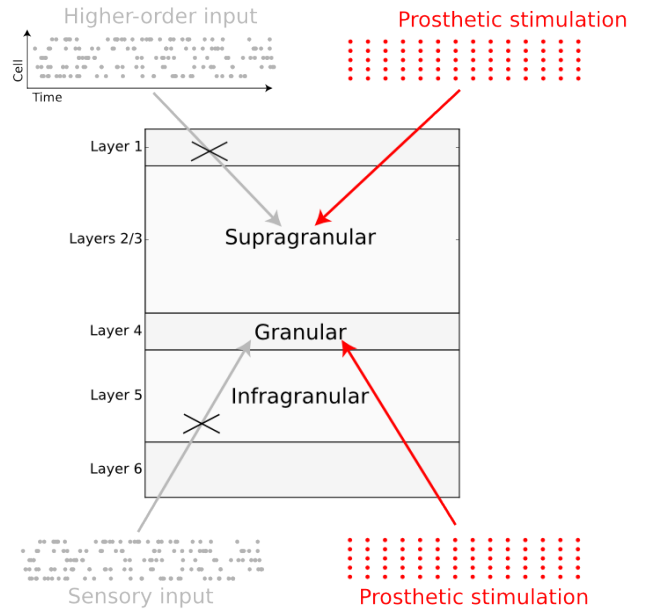


Fig. 1: In the normal brain, excitatory pyramidal cells in the superficial layers (2/3) receive backward input from higher cortical areas, such as those involved with the direction of attention, while the granular layer (4) receives forward input from lower areas (gray lines). This study investigated the effects of reduced input to each layer due to cortical damage elsewhere (black crosses). We then explored normalization of activity patterns through prosthetic stimulation (red lines). In contrast to the original activity (shown in gray), the prosthetic input (red) had only a single frequency and phase.

neuronal populations in total. The numbers and locations of each neuronal population are illustrated in Fig. 2, and are as follows: E2 (i.e., excitatory pyramidal cell of layer 2/3), 1500; I2, 250; I2L, 130; E4, 300; I4, 200; I4L, 140; E5R, 650; E5B, 170; I5, 250; I5L, 130; E6, 600; I6, 250; and I6L, 130. Overall, excitatory neurons outnumber inhibitory ones by a ratio of more than two to one (3220 and 1380 cells, respectively), and almost half the excitatory neurons belong to a single population, E2 (pyramidal cells of layer 2/3).

Individual neurons were modeled as event-driven, rule-based dynamical units with many of the key features found in real neurons, including adaptation, bursting, depolarization blockade, and voltage-sensitive NMDA conductance [11], [12], [13], [14], [15], [16]. Each cell had a membrane voltage state variable (V_m), with a baseline value determined by a resting membrane potential parameter (V_{RMP} , set at either -63 or -65 mV depending on cell type). After synaptic input events, if V_m crossed spiking threshold (V_{TH} , either -40 or -47 mV), the cell would fire an action potential and enter an absolute refractory period, lasting τ_r (either 10 or 50 ms). After an action potential, an after-hyperpolarization voltage state variable (V_{AHP} , either 0.5 or 1 mV) was subtracted from V_m . Then V_{AHP} decayed exponentially (with time constant τ_{AHP} , either 50 or 400 ms) to 0. To simulate voltage blockade,

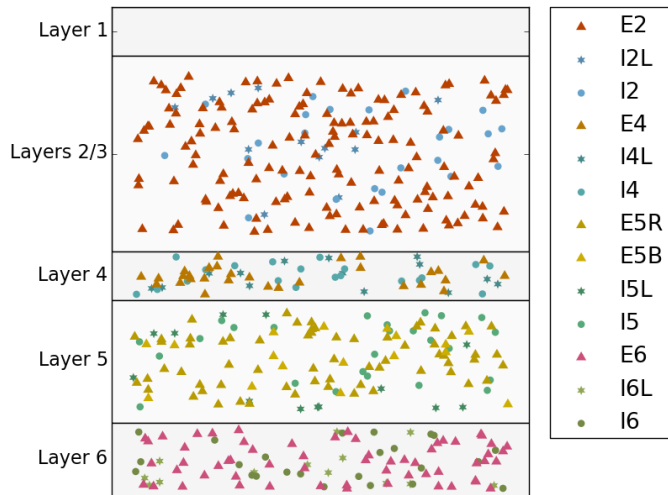


Fig. 2: The structure of the model. Symbols indicate individual neurons (10% of the total shown here), with shape denoting type (triangle = pyramidal neuron; circle = fast-spiking interneuron; star = low-threshold spiking interneuron). The neurons are arranged into six layers; no cell bodies are present in layer 1, and layers 2 and 3 can be considered as a single layer.

a cell could not fire if V_m surpassed the blockade voltage (V_B , either -10 or -25 mV). Relative refractory period was simulated after an action potential by increasing the firing threshold V_{TH} by $W_{RR} \times (V_{block} V_{TH})$, where W_{RR} (either 0.25 or 0.75) was a unitless weight parameter. V_{TH} then decayed exponentially to its baseline value with time-constant τ_{RR} (either 1.5 or 8 ms).

In addition to the intrinsic membrane voltage state variable, each cell had four additional voltage state variables V_s corresponding to synaptic input. These represent AMPA, NMDA, and somatic and dendritic GABA_A synapses. Synaptic inputs were simulated by step-wise changes in V_s , which were then added to the cell's overall membrane voltage V_m . To allow for dependence on V_m , synaptic inputs changed V_s by $dV = W_s(1V_m/E_s)$, where W_s is the synaptic weight and E_s is the reversal potential relative to V_{RMP} . The following values were used for the reversal potential E_s : AMPA, 65 mV; NMDA, 90 mV; and GABA_A, -15 mV. After synaptic input events, the synapse voltages V_s decay exponentially toward 0 with time constants τ_s . The following values were used for τ_s : AMPA, 20 ms; NMDA, 30 ms; somatic GABA_A, 10 ms; and dendritic GABA_A, 20 ms. The delays between inputs to dendritic synapses (AMPA, NMDA, dendritic GABA_A) and their effects on somatic voltage were randomly distributed between 3 and 5 ms, while the delays for somatic synapses (somatic GABA_A) were distributed between 1.8 and 2.2 ms.

Connectivity between the neurons in each of the populations is shown in Fig. 3. Connections tend to be strongest between populations within a given layer; this corresponds to the four “boxes” of high connectivity visible along the diagonal of Fig. 3. Overall, excitatory cells have more projections than in-

hibitory ones, but inhibitory projections are typically stronger; this allows excitation and inhibition to balance, avoiding the two poles of seizures (overexcitation resulting in latch-up) and disappearance of activity (whether from overexcitation or overinhibition). The estimates used for baseline wiring and number of cells per layer were based on published models and anatomical studies [17], [18], [19], [20], [21].

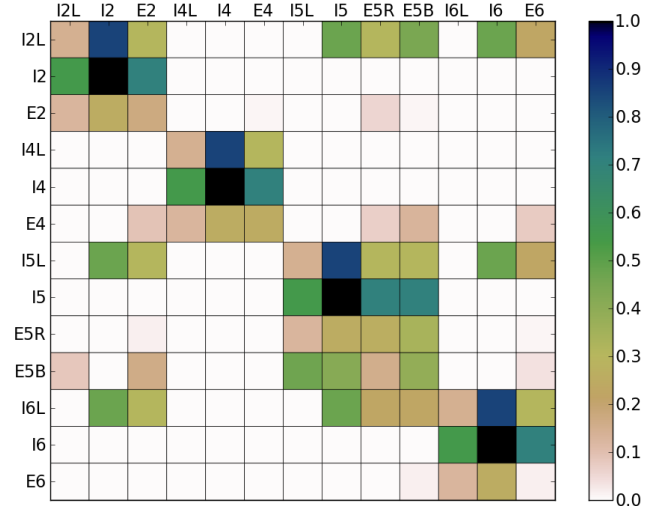


Fig. 3: Connectivity between neuronal populations in the model. Vertical and horizontal axes represent distinct neuronal populations (described in Fig. 2), while color represents the normalized probability that a neuron from a given row will project to a neuron from a given column. The strong but imperfect symmetry about the diagonal of the matrix indicates that most, but not all, connections are reciprocal (e.g., E2 neurons project to I5L neurons, but not vice versa). Most asymmetries result from the fact that excitatory cells tend to project to more distant targets than inhibitory cells.

Additional subthreshold Poisson-distributed spike inputs were used to maintain balanced activity in the model: 100–150 Hz for GABA_A, 240–360 Hz for AMPA receptors, and 40–60 Hz for NMDA receptors. In the present study, these external inputs are not simply included for necessity, but instead are used to explicitly represent the external inputs from other regions of the brain that are lesioned and then replaced. Since cells in the model have one receptor of each type, this represents a total input rate of 380–570 Hz per cell. This input resulted in “spontaneous” firing rates of 0.5–1 Hz in excitatory cells and 1.5–5 Hz in inhibitory cells. Damage was modeled as a 50% reduction in these inputs to either supragranular (layer 2/3) or granular (layer 4) pyramidal cells. The prosthesis consisted of single-frequency, single-phase 100 Hz stimulation of the excitatory cells of the neuronal population with “damaged” input. The frequency was chosen to resemble experimental DBS paradigms (e.g., [22]).

To examine information flow between layers, an additional

low-amplitude spike train signal was applied to layer 4, representing thalamic input. The signal consisted of parathreshold spike inputs (i.e., firing elicited $\sim 30\%$ of the time) to 80% of the pyramidal cells in the stimulated layer. The spike train was generated via a Poisson process with instantaneous probability determined by the amplitude of the experimental thalamic LFP recording described above; the probability was normalized to ensure an average spiking rate of 20 Hz. The exact form of this signal was not crucial to the outcome of the simulations; its primary purpose is to facilitate the causality analysis, since causality is otherwise difficult to determine in a noisy, weakly-connected system.

Simulations were run on NEURON 7.2 [23], [24] for Linux. The full model is available on ModelDB (<http://senselab-med.yale.edu/ModelDB/ShowModel.asp?model=141505>). The model ran for 90 s of simulated time on a CentOS Beowulf cluster with 512 Intel Xeon 2.4 GHz cores; one simulation took approximately 20 minutes to run on a single core.

C. Analysis

Information flow was quantified in terms of spectral Granger causality, also called the directed transfer function [25]. Although many alternative tools for inferring causality exist (e.g., directed transfer entropy [26]), no others allow the spectral properties of the signals to be analyzed in detail. Thus, although spectral Granger causality is limited to detecting linear relationships and by a formal requirement of stationarity, it was felt to be the most informative analysis method in this context.

Spectral Granger causality uses multivariate autoregressive modeling to extend Granger causality formalism to the frequency domain. As in standard Granger causality analysis, spectral Granger causality of $\alpha(f) \rightarrow \beta(f)$ is nonzero if prior knowledge of a variable α at frequency f reduces error in the prediction of β at frequency f . Formally, spectral Granger causality from time series α to time series β is defined as follows [27]:

$$C_{\alpha \rightarrow \beta}(f) = -\log \left(1 - \frac{\left(N_{\alpha\alpha} - \frac{N_{\beta\alpha}^2}{N_{\alpha\alpha}} \right) |H_{\beta,\alpha}(f)|^2}{S_{\beta,\beta}(f)} \right), \quad (1)$$

where $C(f)$ is the spectral Granger causality, N is the noise covariance, $H(f)$ is the transfer function, and $S(f)$ the spectral matrix, as derived from the bivariate autoregressive model of $\alpha(t)$ and $\beta(t)$. This analysis was performed in Python 2.6.5 using code based on the BSMART toolbox (www.brain-smart.org) [27].

III. RESULTS

Reactivation of layer 2/3, using a neuroprosthetic substitution for the missing backward attentional signal, restored full network activation by the forward sensory stimulation (Fig. 4). Baseline activity consisted of fairly constant firing rates among all cell populations (Fig. 4A), with inhibitory

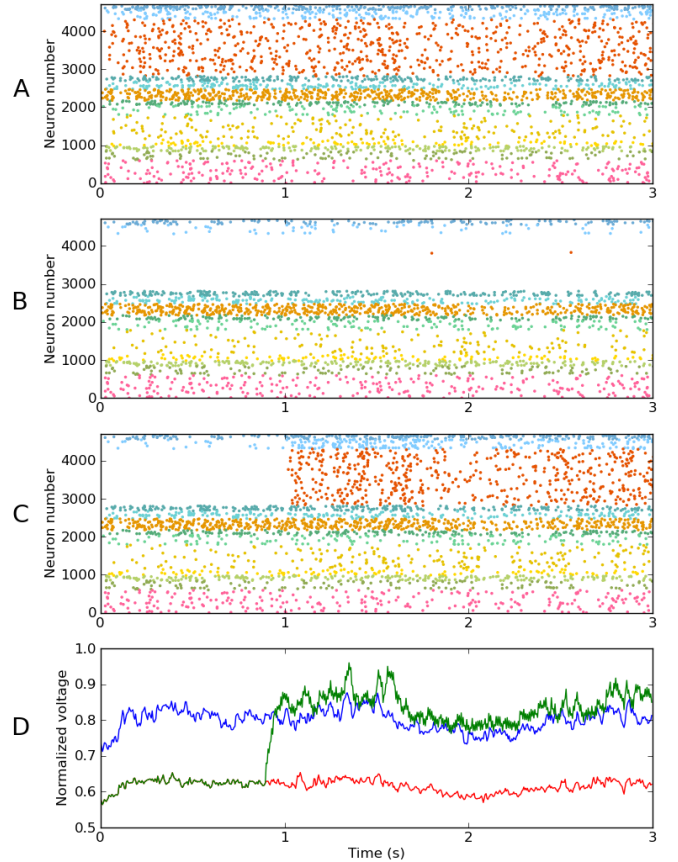


Fig. 4: Restoration of activity after removal of backward (attentional) projections from higher centers to layer 2/3. **A.** Spike raster of baseline activity; different neuronal population types are denoted by color, using the convention defined in Fig. 2. **B.** Removal of backward projections to layer 2/3 produced a marked reduction in number of spikes, especially in the affected layer. **C.** Prosthetic stimulation, initiated 1 s into the simulation, restored activity to baseline levels. **D.** Local field potentials (LFPs) corresponding to each of the three cases: blue, baseline; red, with damage; green, with prosthesis.

populations typically firing at higher rates than excitatory ones, and an average firing rate of 2.5 Hz across all cell populations. The highest firing rate was among E4 cells (7.1 Hz), due to the additional driving signal applied to these cells. I2L cells also showed a high firing rate (7.0 Hz), while the lowest firing rate was among E5R cells (1.2 Hz).

Removal of the backward inputs to layer 2/3 produced an almost total loss of activity in the directly-affected neuronal population, E2 (Fig. 4B). The average firing rate across all populations was reduced by 35% (to 1.7 Hz), with considerable variability between cell populations: the firing rate in I2 cells decreased by 72%, while the firing rate in I6 cells increased by 19%.

The prosthesis successfully restored activity to roughly

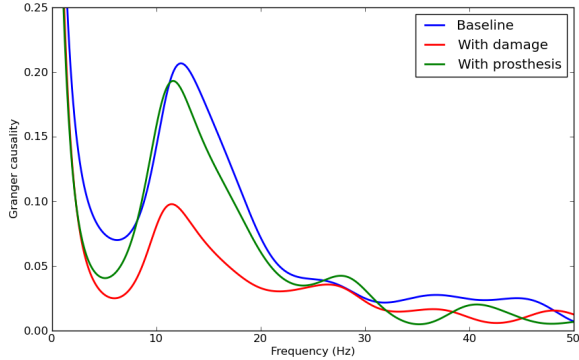


Fig. 5: Spectral Granger causality from layer 4 to layer 5, shown for three cases: baseline (blue), damaged inputs to layer 2/3 (red), and prosthetic stimulation of layer 2/3 (green).

baseline levels (Fig. 4C). The overall firing rate increased to 2.6 Hz, while the E2 firing rate increased from 0.0 to 1.9 Hz (compared to 1.6 Hz for baseline). All other cell population firing rates were restored to within 15% of their baseline values.

Since spiking activity propagates through the network to produce postsynaptic potentials, these changes were clearly visible in the LFPs. The prosthesis restored the overall voltage to baseline levels, but also introduced slightly more variance than was present in the original (Fig. 4D, green line).

Having largely restored activity, we next examined whether this reactivation had functional import, asking whether the restored activity permitted the network to process information normally. We therefore assessed information flow-through of the thalamic signal using spectral Granger causality. Because primary cortical output is from layer 5, we looked at causality from layer 4 to layer 5. These layers were connected not only directly, but also via longer loops, particularly by strong connections through layer 2/3. Note that we were not assessing information flow arising from the prosthetic signal (which is periodic and thus contains little information), or from the background driving signal (which has no structure, and thus contains no useable information). Instead, the information flow was measured from the experimentally-derived forward projection signal into layer 4, which was preserved following damage.

Damage reduced total Granger causality over the frequency range 5–50 Hz to 55% of the original; the prosthesis restored this to 84% (Fig. 5). In addition to restoring lost amplitude of the Granger causality, the prosthesis also restored some of its spectral characteristics: the Pearson correlation between Granger causality spectra for baseline and prosthesis was $r = 0.985$, compared to $r = 0.928$ between baseline and damage. The high correlation values, even between baseline and damage, indicates that the overall magnitude of the Granger causality changed while spectral shape was preserved. Therefore, the reduced input in layer 2/3 did not shift signal filtering by the remaining network.

Firing rates in layers 4 and 5 were not substantially influenced by the damage (changes <0.1 Hz). Therefore, recovery involved restoration of firing organization rather than just restoration of rate. The frequency of the prosthesis had negligible effect on the results, as long as it was sufficiently high (>50 Hz). Stimulation at high frequencies resulted in an effectively stable increase in neuronal excitability, restoring activation of these neurons to the near-threshold level that they had prior to damage. By contrast, if prosthetic stimulation frequency was too low, then neuronal excitability decayed between prosthetic pulses. In this case, out-of-phase signals did not cause the neurons to fire and were lost. The minimum frequency required for the neuroprosthesis (50 Hz) was therefore approximately the reciprocal of the excitatory postsynaptic potential time constants (20–30 ms).

Next, we explored the effectiveness of a prosthesis in repairing damage to cortical inputs to layer 4 (Fig. 6). Layer 4 is the primary site of afferent thalamic input, as well as a major site of forward activation for higher sensory areas. In this case, loss of activation would likely result in a sensory deficit. This scenario was simulated as reduced random synaptic input to E4 cells, while the LFP-derived thalamic signal to the same population remained unchanged. The prosthesis consisted of 100 Hz stimulation of that population.

Both damage and restoration were less dramatic than in the previous example, largely due to the smaller number of neurons in layer 4 compared to layer 2/3 (Fig. 6). In addition, the damaged population (E4) was still receiving thalamic input, which explains why its firing rate decreased by only 49%, as opposed to the nearly 100% loss found after the more extensive E2 input reduction (Fig. 4). This is consistent with the idea that sensory information would be arriving from more than one location: direct thalamic input as well as forward projection from other cortical area. As before, the primary effect of damage to layer 4 was a reduced average firing rate in that layer: from 7.1 Hz to 3.6 Hz (Fig. 6B). The overall firing rate across populations was reduced by 28% to 1.8 Hz. The neuroprosthesis restored the E4 firing rate to 8.1 Hz (114% of the original) and overall firing rate to 2.7 Hz (108% of the original). All other population firing rates were restored to within 10% of their baseline values.

Damage resulted in a 43% reduction in total Granger causality (Fig. 5). The neuroprosthesis restored this to 102% of baseline, almost exactly matching the original. The degree of restoration was manipulable based on the strength of the neuroprosthesis, with increases of information flow to well above baseline produced in other simulations. As before with cortical damage, the neuroprosthesis also restored the spectral shape: the Pearson correlation for baseline vs. neuroprosthesis Granger causality spectra was $r = 0.985$, compared to $r = 0.873$ for baseline vs. damage.

IV. DISCUSSION

We suggest the possibility of achieving substantial improvement in cortical processing with neural prostheses even without restoring information from the lost area. This is due

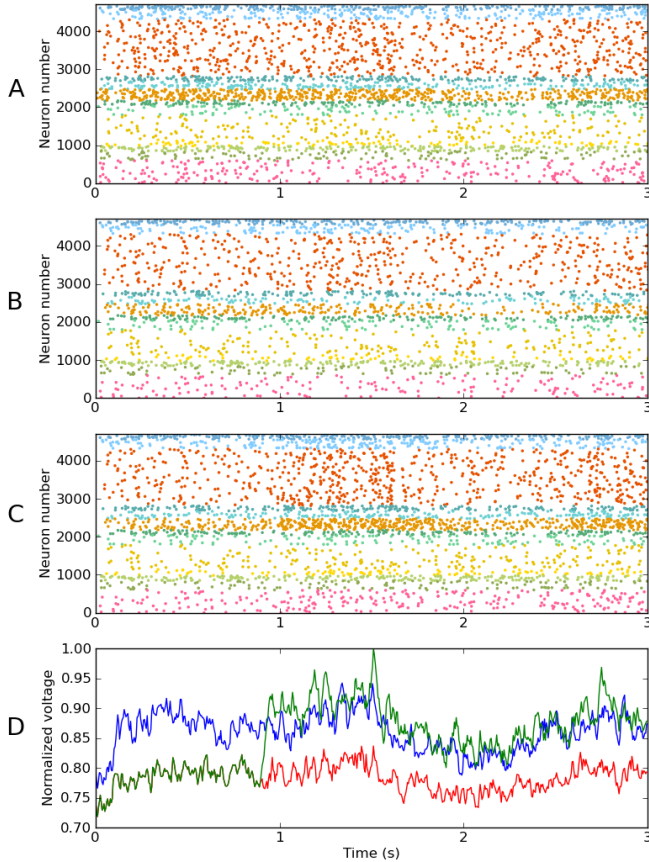


Fig. 6: Restoration of activity after removal of forward (sensory) projections to layer 4. **A.** Spike raster of baseline (identical to Fig. 4A). **B.** Damage of forward activation to layer 4 moderately reduces excitatory activity in all layers but to a lesser extent than in Fig. 4B. **C.** Prosthetic stimulation at 1 s into the simulation restored activity. **D.** LFPs: blue, baseline; red, with damage; green, with prosthesis (note: y-axis scale differs from Fig. 4D).

to the phenomenon of primary diaschisis: given an area A that projects to B , loss of inputs from A will produce disruption of activity in B due to the loss of activation support. The situation is comparable to that of an old crystal radio – the signal provides not only information but also provides the activation required for the unit to function. The difference is that a crystal radio does not multiplex (i.e., it only operates on one signal at a time), so there is nothing else for the radio to do if one restores carrier without restoring signal. In the present case, the prosthesis restores area dynamics without adding back information (in the technical sense, there is Shannon information in the signal we provide, but it does not represent anything). Activity in area B is then restored, making B able to handle other information sources.

The complexity of multiplexing in neocortex is as yet only superficially understood. In sensory systems, two streams of

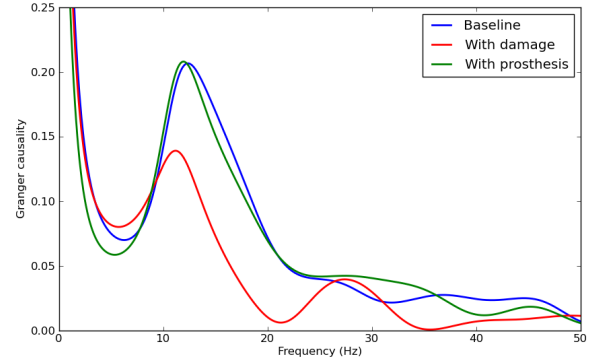


Fig. 7: Spectral Granger causality from layer 4 to layer 5, shown for three cases: baseline (blue), damaged inputs to layer 4 (red), and prosthetic stimulation of layer 4 (green).

information have been identified: a primary stream flowing forward from the afferent influx, and another stream flowing backward to putatively provide attentional and binding guidance for the primary signal processing. We explored these two streams in order to assess to what extent loss of one stream could be patched in order to restore processing of the remaining stream. There are, of course, other information streams in addition to these two. For example, layer 6 receives significant input from thalamic matrix, an input distinct from both thalamic core and from other cortical areas. These different inputs will also be likely to have different statistical patterns, given the different firing patterns of different cell types in the brain. The effect different input patterns have on the model will be related to the model’s multiple transfer functions (input-output relationships). A limitation of the current study is that every cell in the model received Poisson-distributed external inputs with the same statistical properties.

Damage to the forward stream (Fig. 6B) would generally be expected to produce the greater disability. The forward pathways follow linked pathways from a primary sensory area, such as somatosensory (S1), auditory (A1), and visual (V1). Grossly, this path is believed to arise from superficial layers of the source cortical area (layer 2/3) and terminate in deep layers (layers 4-6) of the targeted cortical area. In our simulations, we assumed this termination to be primarily onto layer 4, and reserved layer 5 for use as the output pathway. Since layer 6 receives a major input from thalamic matrix, it did not play a major role in these purely cortical simulations.

Loss of afferent input represents loss of information about the outside world. If this damage is sufficiently early in the system, either in the periphery or in primary sensory cortex, the total loss of sensation (somatosensory anesthesia, deafness or blindness) would likely benefit little from an information-free prosthetic (although the example of blindsight demonstrates that other pathways may provide information even when primary pathways are gone [28]). On the other hand, if the damage was to lower cortical areas – the situation simulated here – one would expect that prosthetic treatment

would be of benefit, since in this case the substantial cross-projections from other areas for the same sensory modality would be expected to help fill in the missing information. The prosthesis would then make this information available by restoring information-processing capacity to the area of primary diaschisis, allowing passage of information from such remaining areas via layer 2/3 to the outputs from layer 5 (Fig. 7).

In these simulations, we observed that causality from layer 4 to layer 5 could be made to significantly exceed the baseline case (data not shown). This was due to the fact that the neuroprosthetic could be made to directly target a particular input stream, and therefore alter the importance of that stream relative to other streams. For example, the replacement of inputs into layer 4 increased its signal-to-noise ratio, resulting in greater predictability (and thus Granger causality) in layer 5.

In contrast to the forward case, loss of the layer 2/3 inputs from the backward projections would preserve primary afferent information (Figs. 4 and 5). Restoration of local processing would restore the ability to process and perceive afferent inputs. Here, the prosthetic stimulation can be seen as providing a continuous attention signal as a replacement for natural, dynamically-modulated attention signals. In addition to temporal information, natural attention signals may have important spatial properties [29], which were also neglected in our simulated prosthesis.

A precise neuroprosthesis would require stimulation of afferents to an area rather than stimulation of the area itself. In this way, the driving signal is delivered to particular cell populations rather than to many different cell populations. In the present case we would suggest that stimulation of superficial cortex (Fig. 4) would best be performed by activation of superficial projections (layer 1) anterior to the area to be reactivated. This would be expected to access afferents projecting to layer 2/3. In the case of missing activity in layer 4, stimulation could be provided to subcortical white matter or thalamus.

V. CONCLUSION

When a cortical area A that influenced area B is damaged, not only is the information that flowed from area A lost, but critical activation that supported the dynamics of B is also lost. In the absence of these normal dynamics, cortical processing in area B will be compromised or even lost – the phenomenon of primary diaschisis. Therefore, the first task of a neural prosthesis is to restore the dynamics and information processing capacity of a cortical area. We have shown here that it may be possible to restore these dynamics using a simple neuroprosthesis.

ACKNOWLEDGMENT

We thank Mingzhou Ding and Jue Mo for assistance with Granger causality calculations, Joseph Lizier for feedback on alternative causality measures, and John Choi and Marcello DiStasio for the description of the experimental procedure.

REFERENCES

- [1] C. von Monakow, *Die Lokalisation im Grosshirn und der Abbau der Funktion durch kortikale Herde*. Wiesbaden: JF Bergmann, 1914.
- [2] J. Reggia, S. Goodall, Y. Shkuro, and M. Glezer, “The callosal dilemma: explaining diaschisis in the context of hemispheric rivalry via a neural network model,” *Neurol Res*, vol. 23, pp. 465–471, 2001.
- [3] J. Meyer, K. Obara, and K. Muramatsu, “Diaschisis,” *Neurol Res*, vol. 15, pp. 362–366, 1993.
- [4] K. G. Lloyd, L. Davidson, and O. Hornykiewicz, “The neurochemistry of Parkinson’s disease: effect of L-dopa therapy,” *J Pharmacol Exp Ther*, vol. 195, no. 3, pp. 453–464, 1975.
- [5] A. Stefani, A. Lozano, A. Peppe, P. Stanzione, S. Galati, D. Tropepi, M. Pierantozzi, L. Brusa, E. Scarnati, and P. Mazzone, “Bilateral deep brain stimulation of the pedunculopontine and subthalamic nuclei in severe Parkinson’s disease,” *Brain*, vol. 130, pp. 1596–1607, 2007.
- [6] D. Rasche, P. Rinaldi, R. Young, and V. Tronnier, “Deep brain stimulation for the treatment of various chronic pain syndromes,” *Neurosurg Focus*, vol. 21, p. E8, 2006.
- [7] S. Shipp, “The importance of being agranular: a comparative account of visual and motor cortex,” *Philos Trans R Soc Lond B Biol Sci*, vol. 360, pp. 797–814, 2005.
- [8] D. Van Essen, C. Anderson, and D. Felleman, “Information processing in the primate visual system: an integrated systems perspective,” *Science*, vol. 255, pp. 419–423, 1992.
- [9] R. Quilodran, M. Gariel, N. Markov, A. Falchier, J. Vezoli, J. Sallet, J. Anderson, C. Dehay, R. Douglas, K. Martin, P. Barone, K. Knoblauch, and H. Kennedy, “Strong loops in the neocortex,” *Society for Neuroscience Abstracts*, p. 853.4, 2008.
- [10] J. Francis, S. Xu, and J. Chapin, “Proprioceptive and cutaneous representations in the rat ventral posterolateral thalamus,” *Journal of Neurophysiology*, vol. 99, pp. 2291–2304, 2008.
- [11] W. Lytton and M. Stewart, “A rule-based firing model for neural networks,” *Int J Bioelectromagnetism*, vol. 7, pp. 47–50, 2005.
- [12] —, “Rule-based firing for network simulations,” *Neurocomputing*, vol. 69, no. 10–12, pp. 1160–1164, 2006.
- [13] W. Lytton and A. Omurtag, “Tonic-clonic transitions in computer simulation,” *J Clin Neurophysiol*, vol. 24, pp. 175–181, 2007.
- [14] W. Lytton, S. Neymotin, and M. Hines, “The virtual slice setup,” *J Neurosci Methods*, vol. 171, pp. 309–315, 2008b.
- [15] W. Lytton, A. Omurtag, S. Neymotin, and M. Hines, “Just-in-time connectivity for large spiking networks,” *Neural Comput*, vol. 20, no. 11, pp. 2745–2756, 2008.
- [16] S. Neymotin, H. Lee, E. Park, A. Fenton, and W. Lytton, “Emergence of physiological oscillation frequencies in a computer model of neocortex,” *Front Comput Neurosci*, vol. 5, no. 19, pp. 1–17, 2011.
- [17] H. Adesnik and M. Scanziani, “Lateral competition for cortical space by layer-specific horizontal circuits,” *Nature*, vol. 464, no. 7292, pp. 1155–1160, 2010.
- [18] T. Binzegger, R. Douglas, and K. Martin, “A quantitative map of the circuit of cat primary visual cortex,” *Journal of Neuroscience*, vol. 24, pp. 8441–8453, 2004.
- [19] S. Lefort, C. Tomm, J.-C. Floyd Sarria, and C. Peterson, “The excitatory neuronal network of the C2 barrel column in mouse primary somatosensory cortex,” *Neuron*, vol. 61, pp. 301–316, 2009.
- [20] S. Neymotin, K. Jacobs, A. Fenton, and W. Lytton, “Synaptic information transfer in computer models of neocortical columns,” *J Comput Neurosci*, vol. 30, no. 1, pp. 69–84, 2011.
- [21] R. Traub, D. Contreras, M. Cunningham, H. Murray, F. LeBeau, A. Roopun, A. Bibbig, W. Wilent, M. Higley, and M. Whittington, “Single-column thalamocortical network model exhibiting gamma oscillations, sleep, and epileptogenic bursts,” *J Neurophysiol*, vol. 93, pp. 2194–2232, 2005.
- [22] N. Schiff, J. Giacino, K. Kalmar, J. Victor, K. Baker, M. Gerber, B. Fritz, B. Eisenberg, J. O’Connor, E. Kobylarz, S. Farris, A. Machado, C. McCagg, F. Plum, J. Fins, and A. Rezai, “Behavioural improvements with thalamic stimulation after severe traumatic brain injury,” *Nature*, vol. 448, pp. 600–603, 2007.
- [23] M. Hines and N. Carnevale, “NEURON: a tool for neuroscientists,” *The Neuroscientist*, vol. 7, pp. 123–135, 2001.
- [24] N. Carnevale and M. Hines, *The NEURON Book*. New York: Cambridge, 2006.

- [25] M. Kaminski, M. Ding, W. Truccolo, and S. Bressler, "Evaluating causal relations in neural systems: Granger causality, directed transfer function and statistical assessment of significance," *Biological Cybernetics*, vol. 85, pp. 145–157, 2001.
- [26] J. Lizier, J. Heinze, A. Horstmann, J.-D. Haynes, and M. Prokopenko, "Multivariate information-theoretic measures reveal directed information structure and task relevant changes in fMRI connectivity," *J Computl Neurosci*, vol. 30, pp. 85–107, 2011.
- [27] J. Cui, L. Xu, S. Bressler, M. Ding, and H. Liang, "BSMART: a Matlab/C toolbox for analysis of multichannel neural time series," *Neural Networks*, vol. 21, pp. 1094–1104, 2008.
- [28] P. Stoerig and A. Cowey, "Blindsight in man and monkey," *Brain*, vol. 120, pp. 535–559, 1997.
- [29] C. Schroeder, A. Mehta, and J. Foxe, "Determinants and mechanisms of attentional modulation of neural processing," *Front Biosci*, vol. 6, pp. 672–84, 2001.